

# Cooperative Multigroup Broadcast 360° Video Delivery Network: A Hierarchical Federated Deep Reinforcement Learning Approach

Fenghe Hu, *Student Member, IEEE*, Yansha Deng, *Member, IEEE*,  
A. Hamid Aghvami, *Fellow, IEEE*,

## Abstract

With the stringent requirement of receiving video from the unmanned aerial vehicle (UAV) from anywhere in the stadium of sports events and the significant-high per-cell throughput for video transmission to virtual reality (VR) users, a promising solution is a cell-free multi-group broadcast (CF-MB) network with cooperative reception and broadcast access points (AP). To explore the benefit of broadcasting user-correlated decode-dependent video resources to spatially correlated VR users, the network should dynamically schedule the video and cluster APs into virtual cells for a different group of VR users with overlapped video requests. By decomposition the problem into scheduling and association sub-problems, we first introduce the conventional non-learning-based scheduling and association algorithms, and a centralized deep reinforcement learning (DRL) association approach based on the rainbow agent with a convolutional neural network (CNN) to generate decisions from observation. To reduce its complexity, we then decompose the association problem into multiple sub-problems, resulting in a networked-distributed Partially Observable Markov decision process (ND-POMDP). To solve it, we propose a multi-agent deep DRL algorithm. To jointly solve the coupled association and scheduling problems, we further develop a hierarchical federated DRL algorithm with scheduler as meta-controller, and association as the controller. Our simulation results show that our CF-MB network can effectively handle real-time video transmission from UAVs to VR users. Our proposed learning architectures is effective and scalable for a high-dimensional cooperative association problem with increasing APs and VR users. Also, our proposed algorithms outperform non-learning based methods with significant performance improvement.

## I. INTRODUCTION

Unmanned aerial vehicle (UAV) systems bring fast and easy accessibility of aerial video capture into our daily life. Although the existing WiFi or Long-Term-Evolution (LTE) technolo-

F. Hu, Y. Deng, and A. H. Aghvami are with King's College London, UK (E-mail:fenghe.hu, yansha.deng, hamid.aghvami@kcl.ac.uk)(Corresponding author: Yansha Deng).

gies can support low-resolution video transmission for flight control, they are not suitable for applications, where many audiences need simultaneous streaming high-resolution videos from UAVs for enhancing viewing experience with virtual reality contents in large sports events. A typical solution is the True View Technology for large sports events introduced by Intel [1]. It enhances the audiences' viewing experience by allowing audiences to customize their viewing angles freely and be immersed in a selected environment with the help of a large camera array distributed around the stadium and head-mounted displays (HMD) for virtual reality (VR) audiences. The captured video from diverse angles is processed into a volumetric video set, which contains real-time content for VR video resources from different angles. However, the angle of view, namely viewpoint, provided by this system is largely limited by fixed cable cameras. To realise the full vision of event enhancing VR video capture, a wireless network is needed to receive, process and transmit the captured  $360^\circ$  VR video from multiple UAVs to massive VR users. However, as shown by Qualcomm [2], [3], the overall capacity requirement for such service from network to VR users can reach  $22Tbps/km^2$  level, which can't be satisfied with existing wireless technologies. Also, this service requires seamless real-time responses to VR users' viewpoint selections, and the newly generated video frames should be successfully transmitted and decoded without noticeable jitter or delay [2], [4].

Existing research on VR video transmission has been mainly focused on reducing the transmission delay via caching and wireless resource allocation [5]–[9]. In [5]–[7], the authors designed a caching algorithm to reduce the transmission delay of VR video resources from the UAVs or cloud server to the VR users with the support of the edge server. By periodically re-arranging the video resource held at the edge server, the requested video resource can be directly transmitted to the VR users from edge server without fetching from the UAVs in real-time to save the overall delay. In [8], the authors optimized the resource allocation for VR video transmission under the consideration of data correlation. With the human factor in the loop, the authors [9] extended [8] by integrating the prediction of VR users' motions prediction into allocation algorithm and reduce the overall delay of the video resource transmission. However, [4], [10] assumed pre-stored independent VR video resource in the form of chunk or image without considering task correlation and video increment decoding schemes. In [6], a scheduling algorithm was applied to manage the processing and transmission of correlated tasks in VR. However, their models are not suitable for our considered scenario with shared volumetric video, where massive VR users are strongly correlated over both content and geometry.

To tackle the real-time VR video transmission from UAVs to a large number of VR users with content request correlation, the broadcasting of the same content to VR users with the same request is shown to be a promising solution [10]. By discretizing the video resources into smaller units, namely, tiles [11], the broadcasting of correlated video resources may largely reduce the bandwidth requirement. However, the limited coverage and inter-cell interference are detrimental to the broadcasting system, especially for cell-edge VR users. To cope with this challenge, one possible solution is the cooperative transmission, which has been proposed in [12]–[15]. By introducing the concept of cooperative transmission into a large scale network. The authors in [13] proposed a cell-free (CF) multi-input-multi-output (MIMO) network to facilitate wide range cooperation among a large number of distributed access points (AP) with cooperative transmission by a central server via high-speed backhaul links. This concept is further extended to user-centric CF-MIMO network, where the APs are clustered into different groups that can serve multiple groups of users simultaneously [14]. It is also shown from [15] that the carefully designed precoding matrix can help to improve the spatial efficiency of user-centric CF network. However, the association problem in [14], [15] is complex to solve with a large number of cooperative APs. The deep reinforcement learning (DRL) has been shown useful in solving caching, scheduling, and association problems dynamically [8], [10]. However, a large number of VR users and cooperative APs introduce a high-dimensional environment (i.e. channel state, actions of multiple AP). Luckily, a convolutional neural network (CNN)-based DRL is known to be able to extract complex wireless features from the environment [16].

Motivated by the above, in this paper, a CF broadcast network is proposed to jointly stream the VR video resources from UAVs and broadcast to the target VR user groups with spatial and content correlation. In this network, there are two challenging problems to solve in real-time: 1) a scheduler to capture the decoding relationship between VR video resources; 2) an association algorithm to dynamically re-groups APs to connect UAVs with each VR user group. Importantly, the scheduling and association stages occur sequentially. More specially, the scheduler first decides the tiles to be transmitted, which corresponds to a UAV that providing this tile in real-time and a VR user group that requested this tile. The locations of each VR user group will then influence the optimal association decision between APs and a VR group to avoid high inter-cell interference and ensure full coverage. This calls for a joint design of scheduling and association algorithms. Our contributions are summarized as follows:

- We first propose a decode-forward (DF) CF-MB network for VR video resource transmis-

sion with *UAV-APs* uplink from UAV camera to APs group, and *APs-VR* downlink from APs group to users. We also define our VR video resource via tiles, and QoE metric via the viewpoint-peak-signal-noise-ratio (V-PSNR) based on the number of successfully decoded tiles at the VR users' sides. Then, we formulate our optimization problem as the maximization of the total V-PSNR in each group of picture (GOP) for all the VR users.

- We then introduce conventional methods for both scheduling and association, which are the popularity-based proportional fair (P-PF) scheduler, and cell-based (CB) and cell-free (CF) association approach, respectively.
- Formulating the association problem as a partially observable Markov-decision-process (POMDP), we first propose a centralized DRL algorithm with CNN layers. With the exponential growth of action space with an increasing number of APs, our results reveal the limitation of scalability in a centralized learning approach.
- To improve the scalability of our algorithm, we decompose the association problem into multiple subproblems, resulting in a networked-distributed Partially Observable Markov Decision Process (ND-POMDP), which are coordinated via mean-field theorem. We propose a federated distributed multi-agent DRL approach with the distributed rainbow agent at each AP. Our results show that our distributed algorithm can efficiently solve the association optimization problem even with a large number of cooperative APs and VR users.
- To handle the interplay between the scheduling and the association, we propose a hierarchical DRL architecture with a centralized scheduler and our proposed multi-agent DRL association to jointly optimize the V-PSNR. Our results show that our proposed hierarchical multi-agent DRL approach can effectively support the cooperation of APs.
- Simulation results show that our proposed three learning-based algorithms can effectively adapt to the dynamic environment with arbitrary density, locations, and request patterns VR users, while significantly outperform non-learning-based conventional approaches.

The remainder of this paper is organized as follows. Section II illustrates the communication model and video decoding model. In Section III, we define our optimization target with defining viewpoint peak signal-noise ratio (V-PSNR) as the QoE metric. We propose conventional methods for scheduling and association separately. In Section IV, we first propose our centralized DRL algorithm for association problem. We introduce ND-POMDP problem, which is then solved a federated multi-agent association setting. Then, in Section V, we apply hierarchical learning

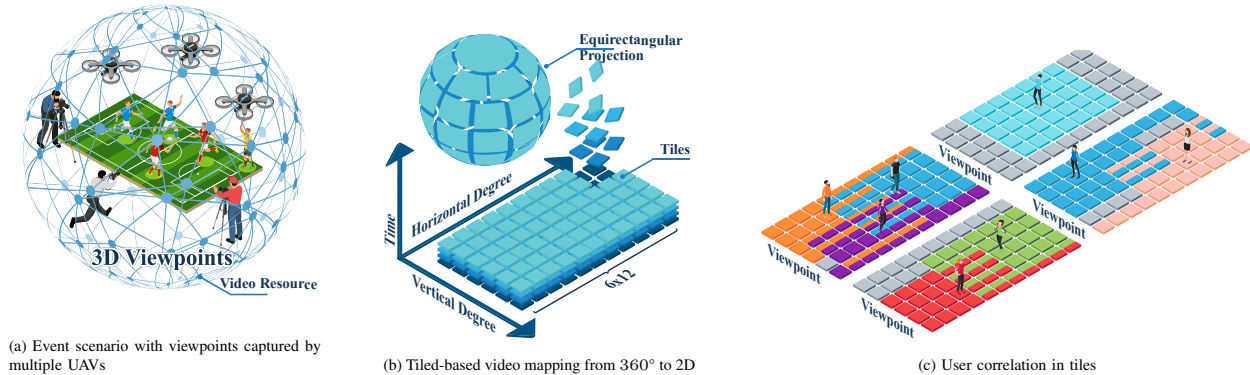


Figure 1: Illustration of scenario, tiled-based video model and corresponding VR user correlation.

method to capture both scheduling and association sub-problems. The numerical results are presented in Section VI. Finally, we conclude the paper in Section VII.

*Notation:* In this paper,  $\mathbb{R}$  is the set of real numbers,  $\mathbb{C}$  is the complex field, and  $\mathbb{1}$  denotes the binary set.  $|\cdot|$  gives the absolute value or number of elements inside a set. Dimensions of vectors/matrices are indicated by format  $M \times N$ .  $H^T$ ,  $H^H$  are the transpose, conjugate transpose respectively, of a matrix  $H$ . The operators  $\mathbb{E}[\cdot]$  denotes expectation.

## II. SYSTEM MODEL

As illustrated in Fig. 1a and Fig. 2, we consider a cell-free multi-group broadcast (CF-MB) network for 360° video transmission in a large sports event. This CF-MB network is composed of 1) a set of APs  $\mathcal{B}$ , which are located in the grid; 2) a central server, which connects all APs through backhaul optical links; 3) a set of randomly located camera UAVs  $\mathcal{U}$ , where each UAV provides the video resource from their orientation; and 4) a set of VR  $\mathcal{V}$  users, whose locations follow Poisson cluster process (PCP) with  $|\mathcal{U}|$  clusters [17]. Each VR user requests video resource from a UAV based on their field-of-view (FOV). As shown in Fig. 1c, the overlapped field-of-view forms correlation among VR users' requests [10]. Considering that the VR users' video requests can correlate to their location in large sports event scenarios, we apply PCP distribution to capture the geographically correlated video requests. We assume that VR users in each cluster request video resources from the same UAV, while the clusters can be overlapped or disjointed. All nodes are located inside the serving area of the plane  $\mathbb{R}^2$ , and remain spatially static for each group-of-picture (GOP) once deployed. The video resource is captured by UAVs, processed by central server, and transmitted to VR users via CF-MB network on request. In short, the CF-MB network acts as a decoded-forward (DF) relay, which receives the video from UAV and broadcasts the processed video to target the VR user group based on VR users' request.

However, the resource requests are small packets in tens of bytes level, whereas the video data's size is usually in GB level. Due to the significant different traffic characteristics of video data and VR request, we focus on the *UAV-APs* uplink from UAVs to the APs in CF-MB network, and the *APs-VR* downlink from the APs in CF-MB network to VR users in this paper.

### A. Transmission Channel Model

To capture the different channel characteristic between APs, UAVs and VR user groups, we consider different channel models for the *UAV-APs* uplink and the *APs-VR* downlink, respectively. The *UAV-APs* uplink from UAV to APs and *APs-UAV* downlink from APs to VR user group occupy  $B_{UL}$  and  $B_{DL}$  bandwidth, respectively. We also assume that a perfect channel state information (CSI) is available at the APs. We assume that both channels follow block fading assumption, where the channel remains constant on a time-frequency coherence block [18].

#### 1) UAV-APs Uplink

The *UAV-APs* uplink between a UAV and a AP group forms a virtual single-input-multi-output (SIMO) system, where multiple APs are associated to enhance the signal reception quality. Considering potential line-of-sight (LoS) and non-line-of-sight (NLoS) for low altitude flying drones, we adopt free-space path loss and Rayleigh fading to model the *UAV-APs* uplink path loss model as

$$h_{u,b} = \begin{cases} \left(\frac{4\pi d_{u,b} f_c^{UL}}{c}\right)^{\alpha_{UL}} \eta_{LoS} \beta_{u,b}, & P_{LoS}^{u,b} \\ \left(\frac{4\pi d_{u,b} f_c^{UL}}{c}\right)^{\alpha_{UL}} \eta_{NLoS} \beta_{u,b}, & P_{NLoS}^{u,b} = 1 - P_{LoS}^{u,b} \end{cases}, \quad (1)$$

where  $\theta_{u,b} = \frac{180}{\pi} \sin^{-1}\left(\frac{h_u}{d_{u,b}}\right)$  is the elevation angle of the drone,  $h_u$  represents the height of flying drone,  $d_{u,b}$  denotes the distance between the  $b$ th AP and the  $u$ th UAV [19],  $f_c^{UL}$  is the uplink channel center frequency,  $\eta_{LoS}$  and  $\eta_{NLoS}$  are the excessive path loss coefficients in LoS and NLoS cases,  $c$  is the light speed, and  $\alpha_{UL}$  is the path loss exponent. In (1), we adopt the LoS probability of the *UAV-APs* uplink as [20]

$$P_{LoS}^{u,b} = \frac{1}{1 + 11.95 \exp(-0.14[\theta_{u,b} - 11.95])}, \quad (2)$$

where  $\theta_{u,b} = \frac{180}{\pi} \times \arcsin\left(\frac{h_u}{d_{u,b}}\right)$ ,  $h_u$  is the flight height of UAV.

Based on (1) and (2), the combined channel between the  $b$ th AP and the  $u$ th UAV can be expressed as

$$h_{u,b} = [P_{LoS}^{u,b} \eta_{LoS} + P_{NLoS}^{u,b} \eta_{NLoS}] \left(\frac{4\pi d_{u,b} f_c^{UL}}{c}\right)^{\alpha_{UL}} \beta_{u,b}, \quad (3)$$

where  $P_{LoS}^{u,b}$  is given in (2).

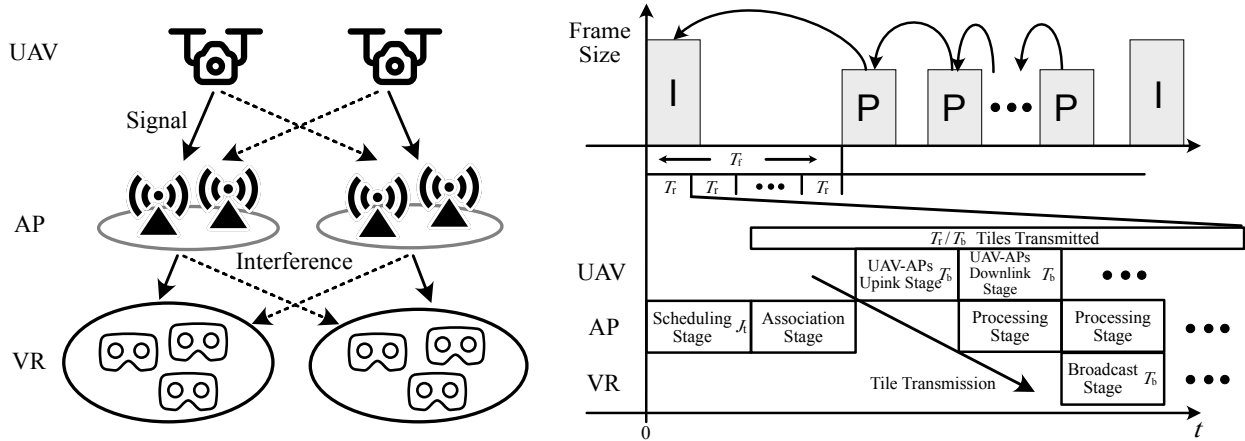


Figure 2: Communication stages and video tiles decoding relationship for considering multi-group-multi-cast system.

## 2) AP-VR Uplink

We consider Rayleigh fading for multi-input-single-output (MISO) transmission between each AP group and VR user [13]. The channel between the  $b$ th AP and  $v$ th VR user is represented as

$$h_{b,v} = d_{b,v}^{-\alpha_{\text{DL}}} \beta_{b,v}, \quad (4)$$

where  $d_{b,v}$  represents the distance between the  $b$ th AP and the  $v$ th VR user,  $\alpha_{\text{DL}}$  represents the AP-VR uplink path loss exponent, and  $\beta_{b,v}$  denotes the Rayleigh small-scale fading.

### B. Video Resource and User Correlation Model

To facilitate effective broadcasting of video resources, it is necessary to split the captured video resource into small tiles, which can be decoded individually. By exploring the nature of video codec, the tiled-based video transmission is introduced for VR video transmission, where the tiles in the same location can be decoded individually [11]. As shown in Fig. 1a, each UAV records a  $360^\circ$  video stream with on-broad camera, which is converted and transmitted in 2D video format via Equirectangular projection. As shown in Fig. 1b, we define that each tile contains color information for  $30^\circ \times 30^\circ$  square in 3D global space [21]. The size of one tile is defined as  $\mu M_T$  bits, where  $\mu$  is the compression rate. We also denote the overall tile set as  $\mathcal{J}$ , which is provided by the set of UAVs  $\mathcal{U}$ . The tiles set generated at time  $t$  is denoted as  $\mathcal{J}_t$ , and the tiles provided by  $u$ th UAV at time  $t$  is denoted as  $\mathcal{J}_t^u$ ,  $u \in \mathcal{U}$ . As shown in Fig. 1b, each UAV provides  $6 \times 12$  tiles.

To describe the content request in each VR user via tiles, we highlight that the field-of-view (FoV) of human is defined as  $210^\circ \times 150^\circ$  [11]. Thus, we have  $5 \times 7$  tiles in one users' request set  $\mathcal{J}_t^v$ ,  $v \in \mathcal{V}$  at time  $t$ , i.e.  $|\mathcal{J}_t^v| = 21$ . The number of tiles can vary based on different positions of viewpoints in  $360^\circ$  space. All VR users' FoV and corresponding tile requests are randomly

generated within the UAV's viewpoint whose required tiles follow the rule of 3D-2D projection [22]. By dividing the VR users' requested video frame into tiles (as shown in Fig. 1c), the VR user group  $\mathcal{V}_j$ , who requests the same tile  $j$  from the  $u$ th UAV, can be served via the broadcast channel at the same time. This highlights the potential benefit of broadcasting overlapping tiles.

### C. Tiles Decoding Model

As shown in Fig. 2, a set of new tiles from video frames with corresponding  $J_t$  tiles are generated every  $T_f$  time, i.e. at frame rate  $1/T_f$ . We assume that all video resources are captured and encoded in the same frame rate and aligned in time.

Considering a dependent frame decoding scheme, as shown in Fig. 2, frames are encoded incrementally within group-of-pictures (GOP) to reduce the overall data rate. For low-latency video encoding scheme, we consider two typical kinds of the frame inside one GOP — intro-coded frame (I Frame), and predicted-coded frame (P frame). The I frame can be decoded individually, whereas the P frame requires the same location's frame or tile in previous time instance to decode [23]. With such dependent encoding scheme, the overall capacity requirement for video transmission can be saved. Thus, one tile can be successfully decoded only when the previous tiles are successfully decoded, whose set is denoted as  $\mathbf{J}_t^v$  in the  $v$ th VR user at time  $t$ .

### D. Network Transmission Procedure

In our considered CF-MB network, the network performs as a DF relay system to support the tile  $j$  transmission from  $u$ th UAV to VR user group  $\mathcal{V}_j$  via APs group  $\mathcal{B}_t^u$ . For time-frequency resource, we adopt time division duplex, which is assumed in many massive MIMO works [24].

As shown in Fig. 2, each frame with a duration of  $T_f$  is divided into  $T_f/T_r$  re-scheduling slots, where  $T_r$  is the length of each re-scheduling slot. Each re-scheduling slot is further divided into  $T_r/T_b$  broadcast slots, where  $T_b$  is the length for each broadcast slot. As shown in Fig. 2, there are 5 stages in each re-scheduling slot of the network transmission procedure, which are scheduling stage, association stage, UAV-APs uplink transmission stage, processing stage, and APs-VR downlink transmission stage. In the scheduling stage, the network first decides the priority of tiles in each UAV based on VR users' requests. Then, the  $\lfloor T_r/T_b \rfloor$  tiles with highest priority in each UAV is picked for transmission within  $T_r$ . As such, the target VR users whose requested tiles are scheduled in  $J_t$  forms the VR user group  $\mathcal{V}_j$  ( $j \in J_t$ ). With the tuples of scheduled tiles, UAV, and target VR user group, each AP selects one tuple to transmit inside each re-scheduling slot  $T_r$ . The single-antenna UAV is capable of transmitting one tile at the



same time. As shown in Fig. 2, this allows for the spatial reuse of frequency resources, where multiple UAVs can be served by different virtual cells at the same time. How to group APs as virtual cells to serve tiles from different UAVs is decided during the association stage.

In the association stage, the network makes association decision by grouping certain APs as a virtual cell  $\mathcal{B}_t^u$  based on their selected tuple of UAV, tiles, and corresponding VR user group. Since the network acts as a DF relay. The association decision determines the APs that support the transmission from UAVs to the VR user groups, i.e. both *UAV-APs* uplink and *APs-VR* downlink. Once the AP is associated with the  $v$ th UAV and  $j$ th tile, it is selected for the tile's reception and broadcasting.

In the *UAV-APs* uplink stage, the  $u$ th UAV transmits the scheduled tile  $j$  to it associated AP group  $\mathcal{B}_t^u$ , which jointly receives the signal. In the processing stage, the tile is processed at the central server, whose delay is considered as a constant value and ignored in our analysis. In the broadcast stage, the APs in virtual cell  $\mathcal{B}_t^u$  jointly broadcast the tile to the VR user group requesting tile  $j$ , i.e.  $\mathcal{V}_j$ . The *UAV-APs* uplink stage, processing stage, and *APs-VR* downlink stage repeated until the end of  $T_r$  using the same scheduling and association decision.

### E. Tile Transmission Model

From the perspective of CF-MB network, the network is operating in full-duplex mode with the transmission of *UAV-APs* uplink and *APs-VR* downlink at the same time over different frequency bands without interfering each other. We assume that all UAV and VR users are equipped with one antenna. Each AP is equipped with two antenna for full-duplex transmission where one antenna for *UAV-APs* uplink, one for *APs-VR* downlink. The tile transmission model can be seen as a DF relay system, where *UAV-APs* uplink is SIMO transmission and *APs-VR* downlink is MISO transmission.

#### 1) The Transmission of *UAV-APs* Uplink

For the SIMO transmission of *UAV-APs* uplink from single UAV to multiple cooperative APs, we adopt the maximum-ratio combining (MRC) technique to realise the multiple reception gain. The received signal  $\gamma_{u^*,b}$  from scheduled the  $u^*$ th UAV to the  $b$ th AP within associated APs group  $\mathcal{B}_t^{u^*}$  at time  $t$  can be expressed as

$$y_{u^*,b} = \underbrace{h_{u^*,b}s_{u^*}}_{\text{Desired signal}} + \underbrace{\sum_{u' \in \mathcal{U}_t \setminus u^*}^U h_{u',b}s_{u'}}_{\text{Interference from Other UAVs'}} + \underbrace{n_0}_{\text{Noise}}, \quad (5)$$

where  $h_{u,b}$  denotes the channel vector from the  $u$ th UAV to the  $b$ th AP,  $\mathcal{U}_t$  is the current scheduled UAV,  $h_{u',b}$  is the interference channel from other interfering UAVs,  $s_u$  is the signal transmitted by the  $u$ th UAV,  $N_0 \sim \mathcal{CN}(0, I_N)$  represents the Gaussian white noise. Then, the signal after MRC can be expressed as

$$\gamma_{u^*, \mathcal{B}_t^u} = \sum_{b \in \mathcal{B}_t^u} w_b y_{u^*, b}, \quad (6)$$

where  $w_b$  is a general weighted MRC scheme with weight  $w_b = h_{u^*, b}^H / \|\mathbf{h}_{u^*, \mathcal{B}_t^u}\|_F$ ,  $b \in \mathcal{B}_t^u$ ,  $\|\cdot\|_F$  represents Frobenius norm, and  $\mathbf{h}_{u^*, \mathcal{B}_t^u} = [h_{u^*, b_0}, \dots, h_{u^*, b_{|\mathcal{B}_t^u|}}]$  is a  $|\mathcal{B}_t^u| \times 1$  channel vector from target the  $u^*$ th UAV to a corresponding APs group  $\mathcal{B}_t^u$  [25].

Thus, the received SINR for tile upload from the  $u$ th UAV to access point group  $\mathcal{B}_t^k$  at time  $t$  can be expressed as

$$\gamma_{u^*, \mathcal{B}_t^u} = \sum_{b \in \mathcal{B}_t^u} p_u |w_b h_{u, b}|^2 / \left( \sum_{b \in \mathcal{B}_t^u} \sum_{u' \in \mathcal{U} \setminus u} p_{u'} |w_b h_{u', b}|^2 + \sum_{b \in \mathcal{B}_t^u} |w_b|^2 \sigma^2 \right). \quad (7)$$

Due to the flat-fading in each broadcast slot, the received data capacity  $D_{u^*, \mathcal{B}_t^u}(t)$  during resource block at the group of APs  $\mathcal{B}_t^{u^*}$  from the  $u^*$ th UAV is given by

$$D_{u^*, \mathcal{B}_t^{u^*}} = T_b B_{UL} \log_2(1 + \gamma_{u^*, \mathcal{B}_t^{u^*}}). \quad (8)$$

## 2) Tile Transmission of the APs-VR Uplink

In APs-VR uplink, the APs form virtual-cells to jointly broadcast the tiles to corresponding VR user groups and enhance the broadcasting quality. As shown in Fig. 2, the cooperative APs can enhance the signal quality in receiving from the VR users, but the inter-cluster interference limits the overall performance. To realise the gain of jointly broadcasting and to improve the worst VR user's performance, we adopt linear sum maximum precoding [26]. With perfect channel state information (CSI), the precoding matrix in the  $b$ th AP can be given by

$$w_b = \alpha_b \sum_v^{\mathcal{V}_t^k} \frac{h_{b,v}^H}{\|h_{b,v}\|^2}, \quad b \in \mathcal{B}_t^k, \quad (9)$$

where  $\alpha_b$  is the normalize factor to ensure  $\|w_b\|_F^2 = 1$ .

Based on (9), the signal received at the selected  $v^*$ th VR user ( $v^* \in \mathcal{V}_t^u$ ) from the  $b$ th AP can

be expressed as

$$\begin{aligned}
y_{\mathcal{B}_t^u, v^*} &= \sum_{b \in \mathcal{B}_t^u} h_{b, v^*} w_b s_b + \sum_{b' \in \mathcal{B} \setminus \mathcal{B}_t^u} h_{b', v^*} w_{b'} s_{b'} + n_{v^*} \\
&= \underbrace{\sum_{b \in \mathcal{B}_t^u} h_{b, v^*} \sum_v \alpha_b \frac{h_{b, v}^H}{\|h_{b, v}\|^2} s_b}_{\text{Desired Signal}} + \underbrace{\sum_{\mathcal{B}_t^n \in \mathcal{B} \setminus \mathcal{B}_t^u} \sum_{b'} h_{b', v^*} \sum_{v'} \alpha_{b'} \frac{h_{b', v'}^H}{\|h_{b', v'}\|^2} s_{b'}}_{\text{Inter-group Interference}} + \underbrace{n_{v^*}}_{\text{Noise}}, \tag{10}
\end{aligned}$$

where  $w_b$  denotes the precoding matrix for the  $b$ th AP in group  $\mathcal{B}_t^u$  at time  $t$ , and  $h_{b, v}$  is the path loss for the channel between the  $b$ th AP and the  $v$ th VR user at time  $t$ .

Based on (10), the SINR from the  $b$ th AP in APs group  $\mathcal{B}_t^u$  to  $v^*$ th VR user in user group  $\mathcal{V}_t^u$  at time  $t$  can be expressed as

$$\gamma_{\mathcal{B}_t^u, v^*} = \sum_{b \in \mathcal{B}_t^u} p_b |h_{b, v^*} w_b|^2 / \left( \sum_{b' \in \mathcal{B} \setminus \mathcal{B}_t^u} p_{b'} |h_{b', v^*} w_{b'}|^2 + \sigma^2 \right). \tag{11}$$

Under given SINR, the received data  $D_{\mathcal{B}_t^u, v}$  in one broadcast slot  $T_b$  from the APs group  $\mathcal{B}_t^u$  to  $v^*$ th VR user can be calculated by the minimum ergodic rate within the broadcast group

$$D_{\mathcal{B}_t^u, v} = T_b B_c^{DL} \log_2(1 + \gamma_{\mathcal{B}_t^u, v^*}). \tag{12}$$

### 3) Overall Capacity

From the whole system point of view, the tiles are delivered to the requesting VR user group via the aforementioned DF network transmission. As the success of tile transmission will only occur when both the *UAV-APs* uplink and *APs-VR* downlink success. The successful transmission of  $j$ th tile can be written as the combination of successful transmission in *UAV-APs* uplink and *APs-VR* downlink as

$$\mathbb{1}[D_{u, v} \geq \mu M_T] = \mathbb{1}[D_{u, \mathcal{B}_t^u} \geq \mu M_T] \wedge \mathbb{1}[D_{\mathcal{B}_t^u, v} \geq \mu M_T], \tag{13}$$

where  $\mu M_T$  is the size of tile to be transmitted,  $\mathbb{1}[x] = 1$  as  $x$  is true,  $\mathbb{1}[x] = 0$ , otherwise.  $\wedge$  is logical and operation.  $\mathbb{1}[x] \wedge \mathbb{1}[y] = 1$  as  $x$  and  $y$  is true,  $\mathbb{1}[x] \wedge \mathbb{1}[y] = 0$ .

### F. Quality-of-experience Metric for VR Users

Generally, for video-based VR service, it is common to define the QoE as the break-in-presence (BIP), which describes the event when users stop responding to the virtual environment [4]. When it comes to our considered video-based VR applications, it is tightly correlated to the video quality. It is common to measure the received amount of information in tiles or frames via the Peak Signal-to-Noise (PSNR) value.

To model the QoE with PSNR value, we jointly consider the transmission and decoding of tiles. We first define the successful decoded tiles at the  $v$ th VR user as set  $\mathbf{J}_t^v$  at time  $t$ . We then refactorize the original PSNR function, which measures the pixel-level information amount, to that of tile-level. By doing so, we can quantify the decoded QoE with PSNR value inside the  $v$ th VR user field-of-view at time  $t$  using viewport-PSNR (V-PSNR) [28] as

$$\text{V-PSNR}_t^v = 10 \log_{10} \left( 1 / \left( 1 + \frac{1}{|\mathcal{J}_t^v|} (|\mathcal{J}_t^v| - \sum_{j \in \mathcal{J}_t^v} \mathbb{1}[j \in \mathbf{J}_t^v]) \right) \right), \quad (14)$$

where  $\mathbf{J}_t^v$  is the decoded tile set, and  $\mathbf{J}_t^v$  represents the actual decoded tiles at time  $t$  in the  $v$ th VR user ( $\mathbf{J}_t^v \subseteq \mathcal{J}_t^v$ ). In (14),  $\sum_{j \in \mathcal{J}_t^v} \mathbb{1}[j \in \mathbf{J}_t^v]$  denotes the number of successfully decoded tiles in  $v$ th VR user at time  $t$ . The V-PSNR value gives  $10 \log_{10} |\mathcal{J}_t^v|$  if all the tiles requested by the  $v$ th VR user are transmitted successfully. The tile  $j$  can be decoded if its and its dependent tiles are successfully transmitted or decoded

$$\mathbb{1}[j \in \mathbf{J}_t^v] = \begin{cases} \mathbb{1}[D_{u,v} \geq \mu M_T], & t < T_f, \\ \mathbb{1}[D_{u,v} \geq \mu M_T] \wedge \underbrace{\mathbb{1}[j' \in \mathbf{J}_t^v]}_{\text{Dependent tile received}}, & t \geq T_f \end{cases}, \quad (15)$$

where  $\mathbb{1}[D_{u,v} \geq \mu M_T]$  is given in (13),  $j$  and  $j'$  are dependent tiles,  $j$  is required to be decoded with  $j'$  incrementally, i.e.  $j$  depends  $j'$  to decode  $j \rightarrow j'$ . In each GOP, when  $t < T_f$ , the tile is from I frame, which can be decoded independently.

### III. PROBLEM FORMULATION AND CONVENTIONAL METHODS

In this section, we defined and decomposed our optimization problem into scheduling and association sub-problems. We then introduce the conventional methods for each sub-problem.

#### A. Problem Formulation

We aim to study how the CF-MB network supports the tile transmission from UAVs to VR users and enhance the QoE of VR users by dynamically adjusting the scheduling and association decisions. Our proposed tile transmission procedure executes each stage successively. In each broadcast slot, the network generates an state  $S_{t_b}$ , which indicates VR users' request, UAVs' position, VR users' V-PSNR, UAV-APs uplink's, APs-UAV downlink's channel information, and etc. The network state  $S_{t_b+1}$  in next broadcast slot is jointly decided by the current system state  $S_{t_b}$ , scheduling tiles  $J_{t_b}$ , and associated virtual cells  $\{\mathcal{B}_{t_b}^u\}$  ( $u \in \mathcal{U}$ ), such that it forms Markov decision process (MDP) problem. In this problem, we denote the scheduling policy as  $\pi_s$  and the association policy as  $\pi_a$ . The scheduler policy  $\pi_s$  is denoted as a weight mapping from the

current state to the priority of tile transmission. The association policy  $\pi_a$  is denoted as the distribution mapping from the current environment state and selected scheduling decisions to the selection of each UAV and corresponding VR user group. Thus, our optimization target can be defined as maximizing the accumulative V-PSNR gain over broadcast slots in  $T_{\text{GOP}}$  via finding the optimal  $\pi_s$  and  $\pi_a$

$$\max_{\pi_s, \pi_a} \mathbb{E} \left[ \underbrace{\sum_{t_b=0}^{T_{\text{GOP}}} \sum_{j \in J_{t_b}} \sum_{v \in \mathcal{V}_j} \Delta \text{V-PSNR}_{t_b}^v}_{\text{V-PSNR Gain in } T_b \text{ for scheduled tile set } J_{t_b}} \right], \quad (16)$$

where the V-PSNR gain is denoted as  $\Delta \text{V-PSNR}_{t_b}^v = \text{V-PSNR}_{t_b}^v - \text{V-PSNR}_{t_b-1}^v$ . However, in tile transmission procedure, the scheduling and the association steps are performed sequentially. In details, the scheduling and association decisions are made in different time steps, i.e. scheduling priority is updated every re-scheduling slot  $T_r$ , and association decision is updated every broadcast slot  $T_b$ . Note that scheduling decision needs to be first updated before the updating of association decision. Another reason for this decomposition is that the joint decision space for both scheduling and association is far complex to be handled via one single algorithm. Thus, we decompose the problem into coupled scheduling and association sub-problems. The scheduling sub-problem acts as a meta-controller to optimize the cumulative intrinsic V-PSNR gain in re-scheduling step  $T_r$

$$\max_{\pi_s} \mathbb{E} \left[ \underbrace{\sum_{t_r=0}^{T_{\text{GOP}}} \sum_{j \in J_{t_r}} \sum_{v \in \mathcal{V}_j} \Delta \text{V-PSNR}_{t_r}^v}_{\text{V-PSNR gain within } T_r} \right]. \quad (17)$$

The association sub-problem maximizes the cumulative extrinsic V-PSNR gain, which is the actual V-PSNR gain for scheduled tile  $J_a$  within  $T_a$

$$\max_{\pi_a} \mathbb{E} \left[ \underbrace{\sum_{t=0}^{T_{\text{GOP}}} \sum_{j \in J_t} \sum_{v \in \mathcal{V}_j} \Delta \text{V-PSNR}_{t_b}^v}_{\text{V-PSNR gain within } T_b} \right], \quad (18)$$

where  $t$  is the system time period index, and  $T$  is the system time period. From (17) and (18), we can observe that the scheduling and association problems are directly coupled, which need to be jointly optimized.

## B. Conventional Approaches

In this section, we introduce conventional scheduling and association approaches for each sub-problem, namely, popularity-based proportional fair (P-PF) scheduling, cell-based (CB), and cell-free (CF) associations, respectively.

### 1) Popularity-based Scheduling

According to (15) and (17), the potential V-PSNR gain for transmitting the tile  $j$  is jointly determined by the number of VR users in the group  $\mathcal{V}_j$ , and the transmission successful rate in current and previous broadcast slots. From (14) and (15), we know that the V-PSNR gain in each broadcast slot  $T_b$  tightly correlates to the number of VR users who request the tile  $j$ , i.e.  $|\mathcal{V}_j|$ . Thus, the more VR users request the tile  $j$ , the more V-PSNR gain via transmitting the tile  $j$ . This instantly results in a popularity-based scheduling algorithm, where tiles with higher popularity are transmitted in each  $T_b$ . Remind that, the scheduling action directly decides which tile to transmit in each broadcast slot for each UAV, which in turn decides and the corresponding VR user group  $\mathcal{V}_j$ .

Additionally, to take decoding state and fairly serve all VR users, we borrow the idea of proportional fair (PF) scheduler that has been widely used in existing cellular network [29]. By adding the previous tiles' decoding state in denominator, the resulting P-PF scheduling method determines the prioritization of tile  $j$  at time  $t_r$  as

$$\text{P-PF}_j = \sum_{v \in \mathcal{V}_j} \mathbb{1}[j \in \mathcal{J}_{t_r}^v, j \notin \mathbf{J}_{t_r}^v] / \left( \sum_{t'=0}^{t_r-1} \mathbb{1}[j_{t'} \in \mathbf{J}_{t'}^v] \right), \quad (19)$$

where  $\mathbf{J}_{t_r}^v$  denotes the successfully decoded tiles in the  $v$ th VR user at time  $t$ , and  $j_{t'}$  denotes the tile at time  $t'$  that is required by tile  $j$ 's decoding, the value of numerator is 1 if current tile is required by  $v$ th VR user, the value of denominator is the sum of previous successfully received tiles, which is required by  $j$  to decode.

### 2) Cell-based and Cell-free Association

We adopt two conventional network schemes to handle the association problem, which are cell-based (CB) and cell-free MIMO (CF) associations: 1) In CB network, each AP is an individual cell, where each AP makes its decision based on its observation independently cooperation. Specifically, each AP is associated with the largest VR user group  $\mathcal{V}_j$ , which has its corresponding  $v$ th UAV and  $j$ th tile ( $j \in \mathcal{J}^v$ ) inside its observation. This scheme may bring high inter-cell interference and poor cell-edge performance; and 2) In CF network, all APs cooperatively receive

one tile in every *UAV-APs* uplink stage and broadcast one tile in the broadcast stage. In another word, all APs are grouped in one virtual cell. In this scheme, the tile with the highest priority among all tiles in all UAVs is selected to be transmitted. This scheme provides high channel capacity for transmitting UAV and corresponding VR users, resulting in inefficient time resource usage with geometry correlated VR users, i.e.  $D_{u,v} \gg \mu M_T$ .

#### IV. REINFORCEMENT LEARNING APPROACH FOR ASSOCIATION

With sequential scheduling and association procedures, we first design a learning-based association algorithm working with conventional P-PF scheduling method to showcase the benefits of learning for the association. Since the geometry-correlated VR users' requests provide another degree-of-freedom in system design, the association algorithm can spatially reuse the frequency resource by grouping APs into virtual cells. To manage the grouping between APs with multiple UAV and hundreds of VR users, it calls for an intelligent algorithm to deal with a complex environment. The conventional intelligent algorithm usually fails to converge. Thus, we introduce deep reinforcement learning (DRL) approaches, which are model-free and shown to be useful in addressing dynamic and temporary dependent control problem in a complex environment [4].

##### A. Centralized Deep Reinforcement Learning

In the following, we propose a centralized DRL approach to find the optimal association policy. Remind that in our considered CF-MB network, the existence of the central server naturally facilitates the centralized DRL approach, where a centralized DRL agent is placed at the central server to make joint association decision for all APs dynamically, to maximize the long-term V-PSNR. Here,  $\mathcal{S}$  ( $s \in \mathcal{S}$ ) is the set of state, and the state  $S_t$  at time  $t$  contains the position of nodes inside the network, channel state information (CSI), VR users' tile request, VR users' decoding state, VR users' V-PSNR value, and UAVs' tile resource state.

Since it is impractical to fully capture the large environment space with massive communicating nodes' channel state and position. Thus, we define our problem as a partially observable MDP (POMDP) problem.

- The observation  $o$  ( $o \in \mathcal{O}$ ) only contains all nodes' position and VR users' tile request without including the UAV and VR users' channel state, due to that the channels are largely dominated by the large-scale fading under APs' cooperative reception and transmission in CF-MB network [13].
- The action  $a$  ( $a \in \mathcal{A}$ ) for the association is a one-hop mapping from each AP to the tuple

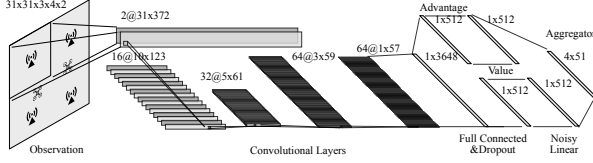


Figure 3: Network Structure of Distributed Association Agent.

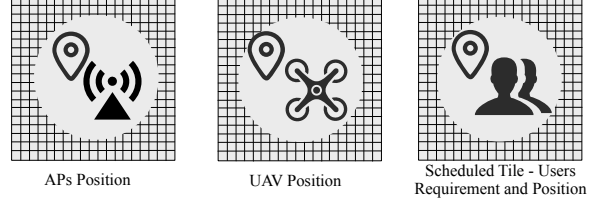


Figure 4: The grid-based observation generated from environment state.

of serving UAV, tile  $j$ , and corresponding VR user group  $\mathcal{V}_j$ . As each AP has  $|\mathcal{U}|$  option to choose, the size of action space of  $\mathcal{A}$  can be calculated as  $|\mathcal{A}| = |\mathcal{U}|^{|\mathcal{B}|}$ , and the action at time  $t$  is denoted as  $A_t$ .

- The reward  $R_t$  ( $R_t = r, r \in \mathcal{R}$ ) is the V-PSNR gain at time  $t$ , designed as

$$R_t = \sum_{v \in \mathcal{V}} \Delta \text{V-PSNR}_t^v, \quad (20)$$

where  $\Delta \text{V-PSNR}_t^v = \text{V-PSNR}_t^v - \text{V-PSNR}_{t-1}^v$ .

It should be noted that network time period is much larger than  $T_b$ , which means the network transmit multiple tiles under one association decision.

### 1) Grid-based Observation and Neural Network Layers

We design a grid-based observation as a fuzzy representation of the state, where the geometry correlated information is mapped into grids. As shown in Fig. 4, for each UAV, three grid-maps correspond to the position of UAVs, APs, and the VR user group requesting the currently scheduled tiles ( $\mathcal{V}_j, j \in J_t$ ). The value in each UAVs and APs grid maps is 1 if the node exists in that grid. For the VR user group grid-map, the value in each grid is the summation number of tile requests from the VR users in that grid, which is normalized into the range of  $(0, 1]$  over the maximum number of tiles' requests in each grid. For example, two VR users from 1th UAV locate in the same grid and request 2 and 3 tiles from scheduled tiles  $J_t$ , the maximum number of tile requests in grids is 8. Then, the normalized value in that grid is 0.625.

To capture the spatial information in grid observations among UAV, AP, and VR users, we introduce convolutional layers to encode the observation into following neural layers. The benefit of applying convolutional layers in communication problems has been shown by previous researches [16]. The convolutional layers can learn to estimate the potential signal and interference. As shown in Fig. 3, we design five layers of convolutional layers and one linear layer to encode the observation into a hidden vector, which is then processed by a duelling network. The duelling network contains two streams composed of two noisy linear layers: advantage and value stream,



respectively. The output from both streams is then aggregated for action decision making [30].

## 2) Rainbow Agent

Known as Rainbow, it is a state-of-the-art DRL approach [30]. It has been shown that the rainbow agent outperforms other DRL approaches in gaming applications. In our problem, the main motivation for applying a rainbow agent is from distributional DRL and state-based noisy layer exploration.

---

### Algorithm 1: Rainbow DRL based APs association.

---

**input** : An environment  $Env$ .

- 1 Initiate network parameters.
- 2 Initiate environment  $Env$ , state  $S_0$  and observation  $O_0$ .
- 3 **repeat**
- 4     **if** Game end **then**
- 5         Obtain  $S_0$  from revising environment  $Reset(Env)$  and set  $t = 0$
- 6     **if**  $t$  can be divided by  $T_r/T_b$  **then**
- 7         Obtain network observation  $O_t$  and scheduled tile set  $J_t$  for current time period from  $Scheduling(S_t)$
- 8     Select an action  $A_t$  greedily:  $A_t = \arg \max_{a \in \mathcal{A}(S_t)} \mathbb{E}[d_t]$
- 9     APs forms virtual cells  $\mathcal{B}_t^u$  based on action  $A_t$
- 10    Tile is transmitted from  $uth$  UAV to corresponding VR users set  $\mathcal{V}^u$  via APs group  $\mathcal{B}_t^u$ .
- 11     $Env$  generates new state  $S_{t+1}$
- 12    Calculate reward  $R_t$  for all VR users
- 13    Push tuple  $(O_t, A_t, R_t)$  to experience replay
- 14    Steps time period index  $t \leftarrow t + 1$
- 15    Train the network parameters by minimising loss defined in (22) with a batch of memories  $(O_{t'}, A_{t'}, R_{t'}, O_{t'+1})$  in experience replay
- 16    Perform a gradient descent for neural network
- 17 **until** Converge

---

In learning procedure at time  $t$ , we first select an current action based on the value estimation of observation  $O_t$  with the policy  $\pi_a$ . We then update the neural network parameters  $\theta$  with actual reward return  $R_t$  (according to (20)) to minimize the estimation error of neural network. However, due to the partial observability and random nature of wireless network, the value of state  $s$  is not a constant number. Thus, the value function can be represented as the expectation over all the instances [31]

$$v_{\pi_a}(o) = \mathbb{E}[v_{\pi_a}(s)|s, o] = \sum_{s \in \mathcal{S}} p(s|o)v_{\pi_a}(s), \quad (21)$$

where  $p(s|o)$  is the limit occupancy probability over the state  $s$  and observation  $o$ . This highlights the importance of estimating the distribution of value return instead of expectation value. With distributional DRL, the value function, which is denoted as  $z(s, o, a)$ , is directly estimated in

distribution form. The value estimation  $d$  generated by the neural network for each action is a discrete mapping from the actual value distribution  $z(s, o, a)$  to a distributive value vector. Each action's value distribution is estimated via  $N_{\text{atom}}$  atoms, where each atom holds its probability mass. We denote the distribution mapping as  $d = (z, p_{\theta}(s, o, a))$ , with probability mass  $p_{\theta}^i(s, o, a)$  on  $i$ th atom. Thus, the action with the highest expectation of the estimated distribution is selected. Then, the network parameters  $\theta$  are updated and optimized by minimizing the Kullbeck-Leibler divergence between the estimated distribution (estimated by neural network with parameter  $\theta$ ) and target distribution  $d_t$  at time  $t$  as [32]

$$D_{\text{KL}}\left(\sum_{k=0}^{n-1} R_{t+k+1} + z, p_{\theta}(S_{t+n}, O_{t+n}, a') \parallel d_t\right), \quad (22)$$

which measures the difference between forward-view  $n$ -step distribution target and current distribution estimation  $d_t$  at time  $t$ , the  $a'$  ( $a' \in \mathcal{A}(S_{t+n})$ ) is the action selected by the policy and estimated distribution from neural network with parameter  $\theta$  and at time  $t + n$ . The loss is minimized with categorical algorithm and gradient descent [33, Algorithm. 1]. The algorithm of association with rainbow agent is presented in **Algorithm. 1**.

To balance exploration and exploitation, we apply noisy nets to perform state-based exploration. As shown in Fig. 3, the noise is added to the linear layers in value and advantage streams, which infers the final estimation to perform state-conditional exploration. With the increasing learning epochs, the network can learn to ignore the noise. In this way, the network automatically balances exploration and exploitation.

### B. Distributed Multi-Agent DRL

It is important to note that the performance of a centralized learning approach is largely limited by the dimension explosion problem caused by increasing serving area and the number of participating APs, i.e. the action space grows exponentially with the number of APs  $|\mathcal{A}| = |\mathcal{U}|^{|\mathcal{B}|}$ . Besides, the transmission, concatenation, and processing of large size observation at the central server cause heavy backhaul overhead.

To address this issue, we divide the association optimization target (18) into sub-problems spatially and solves it via a homogeneous multi-agent setting with the idea of the mean-field theorem [34], [35]. With one agent in each AP, the observation range of each AP is limited due to the fluctuated nature of the wireless signal. First, the wireless signal fades with the increase of communication distance, especially for our considered small APs. The far-side UAVs and APs have limited impacts on the signal gain or interference of the current AP's surrounding

area. Second, without information exchange of the central server, each AP can only receive the surrounding VR users' request and state. Thus, as shown in Fig. 3, we separate the serving area into effective and non-effective areas for each AP and the agent only capture the effective areas, where the effective area contains current AP with its neighbours AP set  $\mathcal{B}^b$ , and is considered as a squared area around AP. The effective areas of different APs are partly overlapped.

With separated serving area, we can formulate our association problem as a networked decentralized partially observable Markov decision processes (ND-POMDP) problem [36], which is a factored version of Decentralized-POMDP problem with mean field theorem [34]. The state space is denoted as  $\mathcal{S}$  ( $s \in \mathcal{S}$ ). The joint action space can be denoted as  $\mathcal{A} = \prod_{b \in \mathcal{B}^b} \mathcal{A}_b$ , where  $\mathcal{A}_b$  is the set of local action space of the  $b$ th AP. Then, the value function for the  $b$ th AP in state  $s$  ( $s \in \mathcal{S}$ ) can be written as the function of joint action space of current AP and its neighbours

$$v_b(s) = \sum_{a_b \in \mathcal{A}_b} \pi_a^b(a_b | s, (\mathbf{a}_{-b})) \mathbb{E}_{a_b, (\mathbf{a}_{-b}) \sim (\pi_a^{-b})} [q_b(s, a_b, (\mathbf{a}_{-b}))]. \quad (23)$$

where  $\mathcal{A}_b$  is the action set of  $b$ th AP,  $\mathbf{a}_{-b}$  present the joint action for  $b$ th AP's neighbors,  $\pi_a^{-b} = \prod_{a_j \in \mathbf{a}_{-b}} \pi_a^{b'}(a_j | s)$  is the joint policy for AP's neighbors,  $\pi_a^{b'}$  is the association policy for  $b'$ th AP ( $b' \in \mathcal{B}^b/b$ ). The Q function for  $b$ th AP is denoted as  $q_b$ . As such, the size of the problem is largely reduced by factorizing the problem as local sub-problem of each AP and its neighbors and treating the rest of APs as part of environment.

Then, we propose a multi-agent DRL approach to solve the ND-POMDP problem. We adopt a rainbow agent at each AP with the same structure as the centralized learning approach, which is explained in **Algorithm. 2**. At the time  $t$ , each AP observes its local observation from state and select an action  $A_t^b$  based on the policy from the neural network. Together with all other APs, after serving UAV and corresponding VR users cooperatively, the  $b$ th AP receives the reward  $R_t^b = \sum_{v \in \mathcal{V}^b} \Delta \text{V-PSNR}_t^v$ , where  $\mathcal{V}^b$  is the VR users in  $b$ th AP's observation range.

However, from (23), we can see that the Q function still depends on  $b$ th AP's neighbors' policy, which is not controllable for current AP. This results in non-stationary environment from the perspective of any individual AP. In this environment, if selecting the action greedily, the action with maximum value usually requires other agents' cooperation. This usually does not hold while all agents selecting their action greedily [34]. Thus, the greedy action selection ignores the need of potential cooperation actions from neighbors, which can easily fail to converge. Thus, we adopt the Boltzmann policy to capture actions with relatively small return, but potentially benefit the overall environment via effective cooperation. The Boltzmann policy for  $b$ th AP in

state  $s$  can be formulated as [34]

$$\pi_a^b(a_b|s, (\mathbf{a}_{-b})) = \exp(-\beta q_b(s, a_b, (\mathbf{a}_{-b}))) / \left( \sum_{a_b \in \mathcal{A}_b} \exp(-\beta q_b(s, a_b, (\mathbf{a}_{-b}))) \right), \quad (24)$$

where  $\beta$  is the temperature for Boltzmann policy,  $q_b(s, a_b, (\mathbf{a}_{-b}))$  is the output of the network.

For our considered cooperation multi-agent system, it has been shown that communication among agents can substantially improve its performance. It is common to share trained policy or parameters among agents to improve cooperative performance [36]. We apply FL via federated average (FedAvg) algorithm to combine useful knowledge from all other APs [37]. The FedAvg algorithm performs averaging every  $T_{\text{federated}}$  time intervals, which is naturally suitable for our network with a central server. Besides, with FL, all agents can be seen as fully cooperative agents with the same optimization target (V-PSNR gain) and global learning model ( $\pi_b = \pi_{b'}, b, b' \in \mathcal{B}$ ). It has been shown that our considered problem can be directly solved using MDP methods with joint action space  $\mathcal{A} = \prod_{b \in \mathcal{B}} \mathcal{A}_b$  of fully cooperative agents and global updated policy in each agent [38]. This guarantees the convergence of our proposing multi-agent algorithm. To enhance the learning performance, we store and train the network with the experience in a concurrent trajectory experience replay, which drops old memories off (produced by old cooperation policies) eventually [39]. The algorithm of distributed learning approach with the federated learning and rainbow agent is represented in **Algorithm. 2**.

## V. HIERARCHICAL LEARNING WITH DEEP REINFORCEMENT LEARNING BASED SCHEDULER

In the transmission procedures, scheduling also plays an important role. It is possible to investigate the benefit of the joint design of the scheduling and association by employing a macro controller at the central server to support the cooperation of APs. By taking the geometry information into account during the scheduling process, we propose a hierarchical reinforcement learning (HRL) approach, which captures primitive scheduler and association sub-problems via a two-level hierarchical structure. This method is shown to be effective for complex environments [40]. As shown in Fig. 6, the scheduling network selects tile set  $J_t$  in the scheduling stage to transmit in the subsequent broadcast slots based on observation. Then, the agent at each AP periodically updates its association decision  $a_b$  based on the environment state  $S_t$  and scheduled decision  $J_t$  at the start of every time step. Following the association decisions, the APs cooperatively transmit the tiles via broadcasting and capture V-PSNR value as the reward.

---

**Algorithm 2:** Hierarchical DRL based joint scheduling and association.
 

---

**input :** An environment  $Env$

- 1 Initiate *scheduling network* and *association network* parameters.
- 2 Initiate environment  $Env$ , state  $S_0$ , and scheduling observation  $O_0^s$ .
- 3 **repeat**
- 4   **if** Game end **then**
- 5     Reset  $Env$  and  $t = 0$ , obtain new  $S_0$ ,  $O_0^s$
- 6   **if**  $t$  can be divided by  $T_r/T_b$  **then**
- 7     Store tuple  $(O_{t-N}^s, A_{t-N}^s, \sum_{t'=t-N}^t R_{t'})$  to scheduling experience replay
- 8     Calculate priority of scheduling  $A_t^s = \mathbb{E}[d_t^s]$
- 9     Select  $T_r/T_b$  tiles with largest priority for each UAV  $J_t = \arg \max(A_t^s, T_r/T_b)$
- 10    Train and update *scheduling network's* parameters with memories in experience replay
- 11   **for**  $b \in \mathcal{B}$  **do**
- 12     Obtain  $O_t^b$  from state  $S_t$ , scheduled tiles  $J_t$  and past state  $S_{t-1}$
- 13     Select an action  $A_t^b$  with (24)
- 14    APs forms virtual cells  $\mathcal{B}_t^u$  for UAVs based on their actions
- 15    Tiles are transmitted from  $u$ th UAV to corresponding VR users set  $\mathcal{V}^u$  via APs group  $\mathcal{B}_t^u$
- 16   **for**  $b \in \mathcal{B}$  **do**
- 17     Calculate reward  $R_t^b$  for VR users in  $b$ th AP's effective area
- 18     Push tuple  $(O_t^b, A_t^b, R_t^b)$  to  $b$ th AP's experience replay
- 19     Train and update *association network's* parameters following the same procedure as Algorithm. 1.
- 20    Step  $Env$  and generates  $S_{t+1}$ .
- 21   **if**  $t$  can be divided by  $T_{federated}$  **then**
- 22     Perform FedAvg among APs  $\mathcal{B}$
- 23 **until** Converge

---

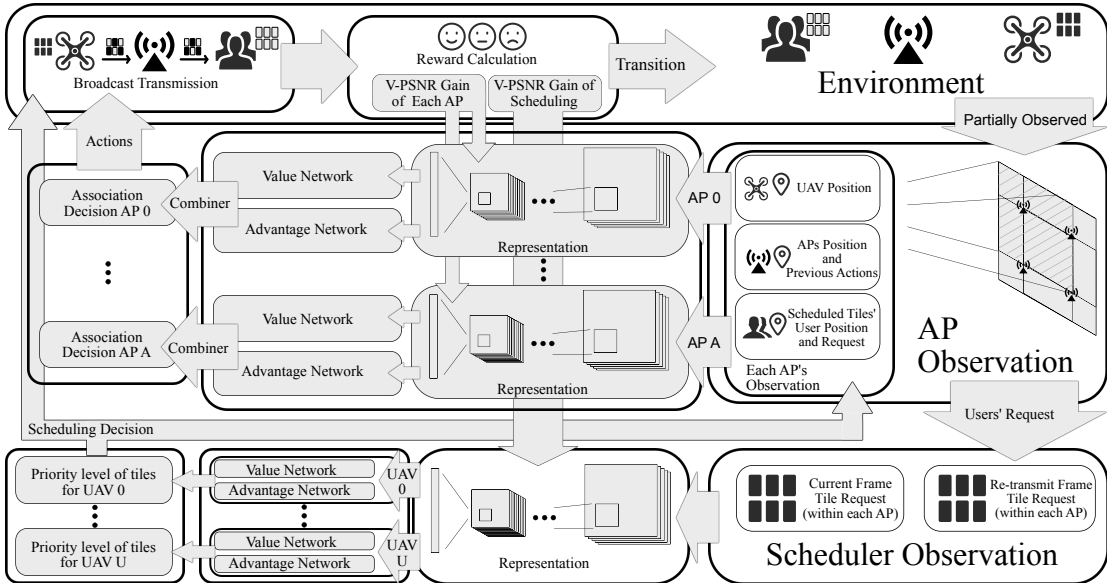


Figure 5: Learning Architecture of Hierarchical Reinforcement Learning

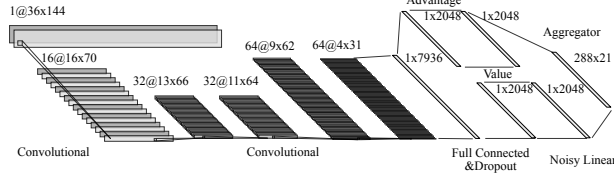


Figure 6: Network Structure of Scheduler Agent in Center Server

Similar as the DRL design in finding the optimal association policy, the scheduling problem is defined as the tuple of state  $\mathcal{S}$ , action  $\mathcal{A}^s$ , policy  $\pi_s$ , reward  $\mathcal{R}$ , and transition  $T_s$  [40]. The state  $s$  ( $s \in \mathcal{S}$ ) follows the same definition in distributed approach. The action  $a_s$  ( $a_s \in \mathcal{A}^s$ ) is the index of tiles, which are selected to be scheduled. The reward follows the same as association part but with  $T_r$  time period:  $\mathcal{R} = \sum_{v \in \mathcal{V}} \Delta \text{V-PSNR}_{t+T_r}^b - \Delta \text{V-PSNR}_t^b$ . Note that scheduling is running at equal or slower time-scale than association, i.e.  $T_r \geq T_a$ . As such, the scheduler acts as meta-controller to estimate the target Q-function

$$q_s^*(s, a_s) = \max_{\pi_s} \mathbb{E} \left[ \sum_{k=t}^{t+N} R_k + \max_{a'_s} q_s^*(s', a'_s) \mid S_t = s, S_{t+N} = s', A_t^s = a_s \right], \quad (25)$$

where  $N$  is the number of system time period before re-scheduling. Similar to the algorithm in Section IV, the target Q-value function of  $b$ th AP's association with scheduler action  $A_t^s$  can be rewritten as

$$\begin{aligned} q_b^*(s, a_b; a_s) &= \max_{\pi_a} \mathbb{E} \left[ \sum_{k=t}^{T_{\text{GOP}}} \sum_{j \in J_k} \sum_{v \in \mathcal{V}_j} \Delta \text{V-PSNR}_k^v \mid S_t = s, A_t^s = a_s, A_t^b = a_b \right] \\ &\stackrel{(a)}{=} \max_{\pi_a} \mathbb{E} \left[ \sum_{j \in J_t} \sum_{v \in \mathcal{V}_j} \Delta \text{V-PSNR}_t^v + \sum_{a'_b \in \mathcal{A}} \pi_a(a'_b \mid s', (\mathbf{a}_{-b})) q_b^*(s', a'_b; a_s) \mid S_t = s, A_t^a = a_b \right]. \end{aligned} \quad (26)$$

We can see that q value functions describe the maximization target of scheduling and association problem in (17) and (18), respectively. The association policy maximizes the intrinsic reward, which is the V-PSNR gain in each broadcast slot. The scheduling policy maximizes the extrinsic reward, which is the potential V-PSNR gain in each re-scheduling slot.

To solve this joint optimization design of scheduling and association problem, as shown in Fig. 5, we apply a similar CNN-based DRL method with a rainbow agent using grid-based observation for scheduling, where the association optimization follows the same design as the distributed DRL approach in Section IV. In the transmission procedures, each AP firstly observe the tile requests and UAVs', APs', and VR users' positions from the environment. The agent of scheduler at a central server then generates its observation based on the returned information from APs. After the transmission based on the scheduling and association decisions. The AP

capture the V-PSNR gain and improve the scheduling and association policy.

With hundreds of tiles and corresponding requests, the observation is composited by the popularity of tiles in  $6 \times 12$  grid from VR users in a small square part of the environment, which is then concatenated into a joint popularity map. To reduce the dimension of observation, we only consider the unsuccessfully transmitted tiles with the highest popularity to be re-transmit without putting all tiles into the observation and action. Each AP observes  $6 \times 12 \times 2$  tiles' popularity for each UAV from its effective state. The overall observation is generated by concatenating each AP's observation. Thus, taking one example, the serving area is separated into  $3 \times 3$  squares. Thus, there are  $3 \times 12$  grid in the horizontal axis and  $3 \times 6 \times 2$  in the vertical axis for each UAV's tiles' request. Then, as shown in Fig. 6, we apply a similar network structure as the agent in Section IV. The  $|\mathbb{J}_t|$  tiles with the highest weight are scheduled and transmitted. The network makes an association decision and transmits tiles. Then, the network is updated with returned V-PSNR gain. The algorithm for hierarchical learning approach is represented in **Algorithm. 2**.

## VI. SIMULATION RESULT

In this section, we examine the QoE of tile streaming from UAV to VR users in our proposed CF-MB network within a squared serving area. The parameter of our simulation and learning system is given in Table. I<sup>1</sup>. In the following, we present the V-PSNR performance for our proposed three learning algorithms in Section VI-A and Section VI-B.

In the simulation, we set the number of VR users as  $|\mathcal{V}| = 120$ , the VR users are distributed following PCP, whose cluster radius is set as  $r_c = 20m$ , the number of UAVs is  $|\mathcal{U}| = 4$ . We set the number of AP as  $|\mathcal{B}| = 9$ , which are located in a  $3 \times 3$  grid with 30 m gap inside the serving area which is  $80m \times 80m$  square. Each AP can observe  $60m \times 60m$  squared effective area surrounding itself. The time period of learning algorithms contains  $10T_b$ , which means the scheduling and association policy is updated after broadcasting 10 tiles.

Note that for a centralized algorithm, due to the large action space of our environment setting ( $|\mathcal{A}| = 4^9$ ), we can't train this oversize model with our devices. Thus, we reduce the environment with only 2 UAV and half broadcast slots compared to the current setting for the centralized algorithm. To ease the presentation of V-PSNR, we normalize the resulting V-PSNR value into  $[0, 5]$  (5 frames in each GOP). Note that, the DRL algorithm is well-known for its lack of

<sup>1</sup>The authors acknowledge the use of the research computing facility at King's College London, Rosalind (<https://rosalind.kcl.ac.uk>).

Parameters	Setting	Radio frequency parameters	Setting
AP-VR link path-loss exponent (AP-VR) $\alpha_{DL}$	4	UAV-AP link path-loss exponent (UAV-AP) $\alpha_{UL}$	2
VR center frequency	5.5 GHz	UAV center frequency	4.5 GHz
Accesspoint grid length	30 m	Drone hovering height	30 m
User density	100	Excessive NLoS Attenuation	20 dB
Accesspoint EIRP	48 dBm	UAV EIRP	48 dBm
Accesspoint transmission bandwidth	5 MHz	UAV transmission bandwidth	5 MHz
Noise power $\theta^2$	-91 dBm	Number of UAV	2
Video parameter	Setting	Learning parameters	Setting
Frame rate	90 Hz	Temperature ( $\beta$ )	100
Group of picture	5 (IPPPP)	Learning rate	$6.25 \times 10^{-5}$
Pixel per degree	60	Dropout rate	0.2
Video compression rate	150	Batch size	32
Frame size ratio (P/I)	0.7	Atoms (Association)	21
User field-of-view	$210^\circ \times 150^\circ$	Atoms (Scheduler)	11
Tile size	$30^\circ \times 30^\circ$	Noisy layer std	0.5
Number of re-schedule between frames $T_f$	28	Discount $\gamma$	1
Broadcast slots between re-schedule $T_r$	10	Multi-step learning	3

Table I: Environment and Learning Parameters.

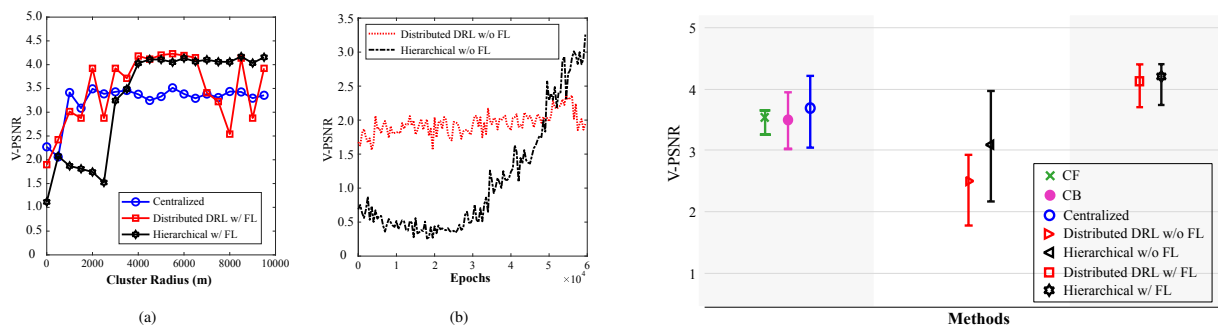


Figure 7: Convergence curves for our proposed algorithms.

Figure 8: V-PSNR Performance of proposing algorithms.

reliability. Average performance is not sufficient to describe the performance of the algorithm. To show the risk of our algorithm [41], we use a standard derivative (SD) error bar to show the performance. We present +std, average performance, and -std, V-PSNR value over 10000 random GOPs with independently generated UAV and VR users. For each algorithm setting, we train  $6 \times 10^4$  epochs and pick the best model during training to plot the result. In the following, we use "Centralized", "Distributed DRL w/ FL", and "Hierarchical w/ FL" to denote the centralized DRL association algorithm with P-PF scheduler, federated distributed DRL algorithm with P-PF scheduler, a hierarchical algorithm with federated distributed DRL and learning-based scheduler algorithm, respectively. To show the effectiveness of FL, we compare two more algorithms: Distributed DRL without FL and Hierarchical FL without FL. For simplicity, we use "Distributed DRL w/o FL" and "Hierarchical FL w/o FL", respectively.

#### A. Overall Convergence and Analysis

Fig. 7 plots the overall V-PSNR versus the training epochs. In Fig. 7a, we observe that the Centralized, Distributed DRL w/ FL and Hierarchical w/ FL converge fast within 10,000 epochs.



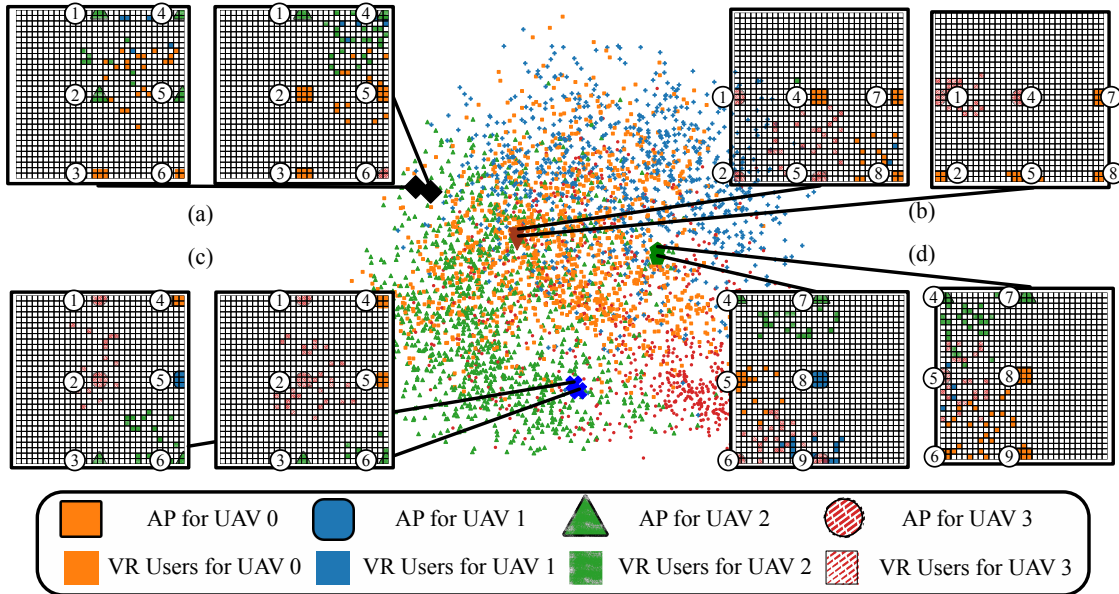


Figure 9: t-SNE embedding of the representations with the learned policy.

Because the FL method combines the learning experience among APs for our fully cooperative association problem. In Fig. 7b, we observe that the Distributed DRL w/o FL fails to converge, whereas the Hierarchical w/o FL approach do converge but requires far more epochs. This is because the Distributed DRL w/o FL approach treats other agents as part of the environment, and the highly dynamic environment makes it fail to converge. In the Hierarchical w/ FL approach, the agent of scheduler acts as a meta-controller, who helps the distributed DRL agents to cooperate. Fig. 8 plots the overall V-PSNR values of different learning algorithms. we observe that the average V-PSNR of algorithms follows: Hierarchical w/ FL  $\approx$  Distributed DRL w/ FL  $>$  CB  $\approx$  CF  $\approx$  Centralized  $>$  Hierarchical w/o FL  $>$  Distributed DRL w/o FL. We observe that CF association provides the V-PSNR with the lowest standard derivation among all algorithms, due to the fully cooperative APs enhance the transmission channel. We observe that Centralized learning obtains worse result compared to Distributed DRL w/ FL and Hierarchical w/ FL algorithm. The reason is that the model is not sufficient for large action space ( $2^9$ ).

In Fig. 9, we show the principle of the proposed neural network by visualising the output of CNN and the final policy. The figure is generated by letting the Distributed DRL agents play for 1000 randomly generated GOPs. With generated vectors from the output of CNN layers, we apply a technique developed for the visualization of high-dimensional data called “t-SNE” to calculate the distance between vectors. Then, the principle composition analyses (PCA) is performed on the vectors to reduce the dimension to 2D space and visualise them in Fig. 9.

Each point is coloured according to the association decisions [42]. In this way, the point cloud in the center presents the learned policy in our model.

Apart from the policy point cloud in Fig. 9, we also randomly present four observations together with their most similar observations by picking the nearest one according to the result of the t-SNE algorithm. Each observation is observed by the AP in the center, which is represented as a grid-map. In each grid-map, the colours in grids represent the position of VR users and their corresponding UAV. The position of APs is also marked and coloured by its association decision from current observation. To ease the reading of these figures, we number the 9 APs in our simulation with numbers from 1 – 9 based on their relative positions. In (a), the grid-maps are observed by 2nd AP. In left grid-map, we can see that 2nd and 5th AP is jointly associated to serve 2nd UAV. In right grid-map, 2nd, 5th APs jointly serve 0th UAV. In (b), the 4th APs forms virtual cells with 7th and 8th APs cooperatively to serve 0th UAV in left grid-map. In right grid-map, 4th and 1st APs jointly serve 3th UAVs. In (c), the 1st and 2nd APs jointly serve the surrounding VR user groups, which request tiles from 3rd UAV. In (d), the left observation from 8th AP shows that it fails to cooperate with 9th AP to serve 2nd UAV and corresponding VR user group. This highlights the fact that the value of the actions in each agent is jointly decided by its and its neighbours' actions in the multi-agent system. The right observation shown that 6th, 8th, and 9th APs jointly serve 0th UAV, whereas the 4th and 7th APs jointly serve 2th UAV.

### B. *Quality-of-experience Analysis*

In this subsection, we plot the V-PSNR value using VR users of three learning algorithms, including Centralized, Distributed DRL w/ FL, and Hierarchical w/ FL, together with two conventional algorithms (CB, CF) in different scenarios.

Fig. 10 plots the V-PSNR value versus the number of VR users. We observe that all algorithms' V-PSNR stay nearly unchanged with increasing numbers of VR users in CF-MB network. This matches our expectation for CF-MB network, where the UAV-APs cooperative reception enhance the received signal from UAV and the APs-VR broadcasting is not sensitive to the number of receiving VR users. It is worth to mention that we only train a single model using random VR users and obtain similar results with different numbers of VR users setting, which shown the scalability of our learning algorithms.

Fig. 11 plots the V-PSNR value versus the VR users' cluster radius. We first see that the V-PSNR value of CF association algorithm keeps the same for different cluster radius, as all APs jointly serve one UAV and corresponding VR user group in the CF association without

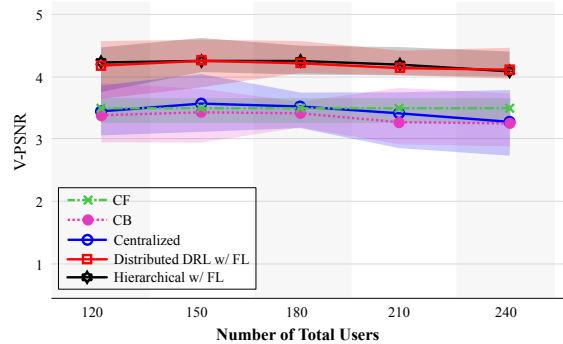


Figure 10: V-PSNR of our proposing algorithms with different number of VR users.

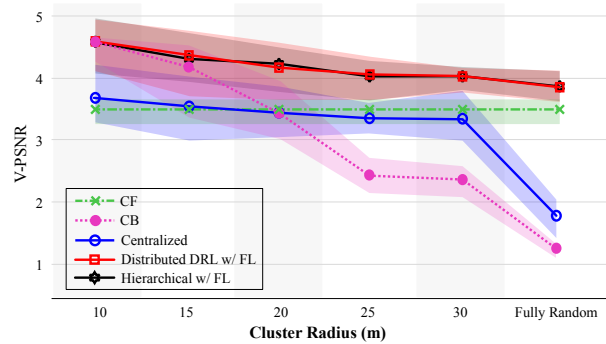


Figure 11: V-PSNR of our proposing algorithms with different VR users' cluster radius.

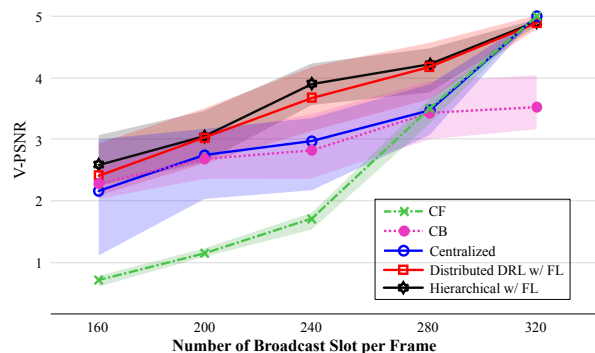


Figure 12: V-PSNR of our proposing algorithms with different broadcast slots in each frame duration.

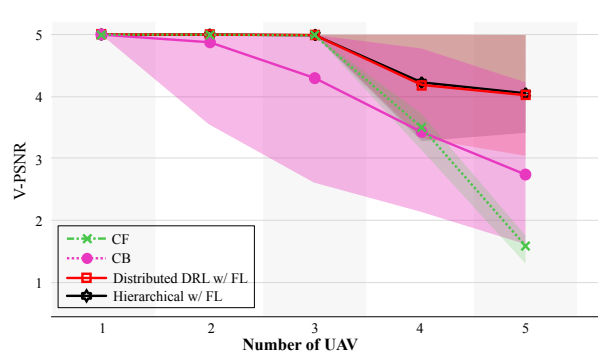


Figure 13: V-PSNR of our proposing algorithms with different number of UAVs.

interference. The CF-MB network provides uniform services in this case. We observe that the V-PSNR of CB association algorithm drops dramatically with the increasing cluster radius. The reason is that increasing cluster radius can lead to more overlap clusters, which calls for cooperation among APs to reduce the inter-cell interference. The CB association fails to serve VR users due to its high inter-cell interference and poor cell-edge performance. We also see that the centralized learning approach fails to converge within our limited number of epochs with random VR users due to the lack of environment resolution with small size network structure. We observe that the V-PSNR value of our proposed distributed algorithms, including Distributed DRL w FL and Hierarchical w FL, drop slightly with the increasing cluster radius, but outperform other algorithms (CF, CB, Centralized).

Fig. 12 plots the V-PSNR versus the number of broadcast slots, which also reveals the slot utilization of our proposed algorithms. Remind that in our considered environment, 4 UAV holds 288 tiles in total. If we set large  $T_b$  and fewer broadcast slots, then two tiles should be fully transmitted successfully within one broadcast slot (160 slots). If we set small  $T_b$  (more broadcast slots), each tile can occupy one broadcast slot individually (320 slots). We observe that the V-

PSNR of CF association method increases with the number of broadcast slots, as the chances of transmission increase. We also observe that the V-PSNR value of CB association approach decrease with the increasing of broadcast slots. The reason is that high inter-cell interference results in low cell-edge performance. We highlight that the V-PSNR value of learning-based algorithms is higher than CB and CF. And the Distributed DRL w FL and Hierarchical w FL outperform the Centralized approach with all different number of broadcast slots.

Fig. 13 plot the V-PSNR value of different algorithm versus the increasing number of UAV. We observe that V-PSNR of CF and CB decreases with the increasing number of UAV due to the lack of resources. We also see that the learning-based algorithms still outperform conventional methods. It achieves high utilization for each broadcast slot with increasing UAV number in both average and standard derivation of V-PSNR. It should be noted that the training complexity of learning algorithms increases linearly with the increasing number of UAV in our network design.

## VII. CONCLUSION

In this paper, we introduced a cell-free multi-group broadcast network for real-time VR video transmission from UAVs to VR users for experience enhancement in a sports event. To optimise the quality-of-experience of VR users with dependent decoded video resources and correlated VR users, we highlighted the importance of the scheduling video tiles and the dynamical association of APs. We also shown that a joint design is needed for correlated and sequential scheduling and association procedures. We first introduced a conventional popularity-based scheduler, and cell-based and cell-free association algorithms to solve each sub-problem individually. To explore the learning-based dynamic association algorithm, we then propose a centralized and multi-agent deep reinforcement learning algorithm, which captures the environment via convolutional layers. To jointly solve the coupled association and scheduling algorithm, we further developed a hierarchical algorithm with scheduler as meta-controller and association algorithm as the controller. Our results demonstrated that both distributed APs and hierarchical with federated learning algorithms can effectively handle a large number of APs and VR users and outperform the centralized algorithm and non-learning-based approach with different environment settings.

## REFERENCES

- [1] Intel, "Intel® True View - Intel in Sports," 2020. [Online]. Available: <https://www.intel.co.uk/content/www/uk/en/sports/technology/true-view.html>
- [2] F. Hu, Y. Deng, W. Saad, M. Bennis, and A. H. Aghvami, "Cellular-Connected Wireless Virtual Reality: Requirements,

- Challenges, and Solutions,” *IEEE Commun. Mag.*, vol. 58, pp. 105–111, May 2020.
- [3] Qualcomm Technologies. Inc., “VR and AR Pushing Connectivity Limits,” Qualcomm., Tech. Rep., 2018. [Online]. Available: <https://www.qualcomm.com/invention/extended-reality/virtual-reality>
- [4] Z. Chen, E. Bjornson, and E. G. Larsson, “Dynamic Resource Allocation in Co-Located and Cell-Free Massive MIMO,” in *IEEE Trans. Green Commun. Netw.*, vol. 4, no. 1. Institute of Electrical and Electronics Engineers Inc., Mar. 2020, pp. 209–220.
- [5] M. Chen, W. Saad, and C. Yin, “Deep Learning for 360° Content Transmission in UAV-Enabled Virtual Reality,” in *53rd ICC 2019*, Shanghai (China), May 2019, pp. 1–6.
- [6] X. Yang, Z. Chen, K. Li, Y. Sun, N. Liu, W. Xie, and Y. Zhao, “Communication-constrained mobile edge computing systems for wireless virtual reality: Scheduling and tradeoff,” *IEEE Access*, vol. 6, pp. 16 665–16 677, Mar. 2018.
- [7] S. Sukhmani, M. Sadeghi, M. Erol-Kantarci, and A. E. Saddik, “Edge Caching and Computing in 5G for Mobile AR/VR and Tactile Internet,” *IEEE Multimed.*, pp. 1–1, Nov. 2018.
- [8] M. Chen, W. Saad, C. Yin, and M. Debbah, “Data Correlation-Aware Resource Management in Wireless Virtual Reality (VR): An Echo State Transfer Learning Approach,” *IEEE Trans. Commun.*, Feb. 2019.
- [9] X. Hou, J. Zhang, M. Budagavi, and S. Dey, “Head and body motion prediction to enable mobile vr experiences with low latency,” in *38th GLOBECOM 2019*, Waikoloa, Dec. 2019, pp. 1–7.
- [10] C. Perfecto, M. S. Elbamby, J. D. Ser, and M. Bennis, “Taming the Latency in Multi-user VR 360: A QoE-aware Deep Learning-aided Multicast Framework,” *IEEE Trans. Commun.*, vol. 68, no. 4, Apr. 2020. [Online]. Available: <http://arxiv.org/abs/1811.07388>
- [11] 3GPP, “3GPP TS 26.247 Progressive Download and Dynamic Adaptive Streaming over HTTP (3GP-DASH),” 2018.
- [12] X. Ge, L. Pan, Q. Li, G. Mao, and S. Tu, “Multipath Cooperative Communications Networks for Augmented and Virtual Reality Transmission,” *IEEE Trans. Multimed.*, vol. 19, no. 10, pp. 2345–2358, Jul. 2017.
- [13] H. Q. Ngo, A. Ashikhmin, H. Yang, E. G. Larsson, and T. L. Marzetta, “Cell-Free Massive MIMO Versus Small Cells,” *IEEE Trans. Wirel. Commun.*, vol. 16, no. 3, pp. 1834–1850, Jan. 2017.
- [14] S. Buzzi and C. D’Andrea, “Cell-free massive MIMO: User-centric approach,” *IEEE Wireless Commun. Lett.*, vol. 6, no. 6, pp. 706–709, Dec. 2017.
- [15] S. Buzzi, C. D’Andrea, and C. D’Elia, “User-centric cell-free massive MIMO with interference cancellation and local ZF downlink precoding,” in *15th ISWCS 2018*. Lisbon, Portugal: IEEE, Aug. 2018, pp. 1–5.
- [16] W. Cui, K. Shen, and W. Yu, “Spatial Deep Learning for Wireless Scheduling,” *IEEE J. Sel. Areas Commun.*, vol. 37, no. 6, pp. 1248–1261, Jun. 2019.
- [17] C. Saha, M. Afshang, and H. S. Dhillon, “Poisson cluster process: Bridging the gap between PPP and 3GPP HetNet models,” in *2017 ITA*. San Diego: IEEE, Feb. 2017, pp. 1–9.
- [18] A. Karimi, K. I. Pedersen, N. H. Mahmood, J. Steiner, and P. Mogensen, “5G Centralized Multi-Cell Scheduling for URLLC: Algorithms and System-Level Performance,” *IEEE Access*, vol. 6, pp. 72 253–72 262, Nov. 2018.
- [19] M. Mozaffari, W. Saad, M. Bennis, and M. Debbah, “Mobile Unmanned Aerial Vehicles (UAVs) for Energy-Efficient Internet of Things Communications,” *IEEE Trans. Wirel. Commun.*, vol. 1, no. 11, pp. 7574–7589, Nov. 2017.
- [20] —, “Unmanned Aerial Vehicle with Underlaid Device-to-Device Communications: Performance and Tradeoffs,” *IEEE Trans. Wirel. Commun.*, vol. 15, no. 6, pp. 3949–3963, Feb. 2016.
- [21] M. Zink, R. Sitaraman, and K. Nahrstedt, “Scalable 360° Video Stream Delivery: Challenges, Solutions, and Opportunities,” *Proc. IEEE*, vol. 107, no. 4, pp. 639–650, Apr. 2019. [Online]. Available: <https://ieeexplore.ieee.org/document/8643410/>
- [22] A. Xu, X. Chen, Y. Liu, and Y. Wang, “A Flexible Viewport-Adaptive Processing Mechanism for Real-Time VR Video Transmission,” in *2019 IEEE Int. Conf. Multimed. Expo Work.*, Shanghai (China), Aug. 2019, pp. 336–341.

- [23] ITU, “H.265: High efficiency video coding,” 2020. [Online]. Available: <https://www.itu.int/rec/T-REC-H.265>
- [24] J. Flordelis, F. Rusek, F. Tufvesson, E. G. Larsson, and O. Edfors, “Massive MIMO Performance—TDD versus FDD: What Do Measurements Say?” *IEEE Trans. Wirel. Commun.*, vol. 17, no. 4, pp. 2247–2261, Feb. 2018.
- [25] N. Jindal, J. G. Andrews, and S. Weber, “Multi-antenna Communication in Ad Hoc Networks: Achieving MIMO Gains with SIMO Transmission,” *IEEE Trans. Commun.*, vol. 59, no. 2, pp. 529–540, Dec. 2011.
- [26] J. Joung, H. D. Nguyen, P. H. Tan, and S. Sun, “Multicast linear precoding for MIMO-OFDM systems,” *IEEE Commun. Lett.*, vol. 19, no. 6, pp. 993–996, Apr. 2015.
- [27] E. Björnson, Ö. Özdogan, and E. G. Larsson, “Intelligent Reflecting Surface versus Decode-and-forward: How Large Surfaces Are Needed to Beat Relaying?” *IEEE Wirel. Commun. Lett.*, vol. 9, no. 2, pp. 244–248, Oct. 2019.
- [28] C. Li, M. Xu, L. Jiang, S. Zhang, and X. Tao, “Viewport Proposal CNN for 360° Video Quality Assessment,” in *IEEE Conf. Comput. Vis. Pattern Recognit.*, Long Beach, CA, Jun. 2019.
- [29] R. Margolies, A. Sridharan, V. Aggarwal, R. Jana, N. K. Shankaranarayanan, V. A. Vaishampayan, and G. Zussman, “Exploiting Mobility in Proportional Fair Cellular Scheduling: Measurements and Algorithms,” *IEEE/ACM Trans. Netw.*, vol. 24, no. 1, pp. 355–367, Feb. 2016.
- [30] M. Hessel, J. Modayil, H. Van Hasselt, T. Schaul, G. Ostrovski, W. Dabney, D. Horgan, B. Piot, M. Azar, and D. Silver, “Rainbow: Combining Improvements in Deep Reinforcement Learning,” in *32nd AAAI 2018*. AAAI press, Oct. 2018, pp. 3215–3222.
- [31] T. Jaakkola, S. P. Singh, and M. I. Jordan, “Reinforcement learning algorithm for partially observable Markov decision problems,” in *Adv. Neural Inf. Process. Syst.*, 1995, pp. 345–352.
- [32] M. G. Bellemare, W. Dabney, and R. Munos, “A Distributional Perspective on Reinforcement Learning,” *34th ICML 2017*, vol. 1, pp. 693–711, Jul. 2017. [Online]. Available: <http://arxiv.org/abs/1707.06887>
- [33] F. Meire, G. A. Mohammad, P. Bilal, and etc, “Noisy networks for exploration,” in *ICLR 2018*, Vancouver (Canada), 2018.
- [34] Y. Yang, R. Luo, M. Li, M. Zhou, W. Zhang, and J. Wang, “Mean Field Multi-Agent Reinforcement Learning,” *arXiv preprint arXiv:1802.05438*, Feb. 2018. [Online]. Available: <http://arxiv.org/abs/1802.05438>
- [35] H. Shiri, J. Park, and M. Bennis, “Communication-efficient massive UAV online path control: Federated learning meets mean-field game theory,” *arXiv preprint arXiv:2003.04451*, 2020. [Online]. Available: <http://arxiv.org/abs/2003.04451>
- [36] N. Ranjit, V. Pradeep, T. Milind, and Y. Makoto, “Networked distributed POMDPs: a synthesis of distributed constraint optimization and POMDPs,” in *AAAI’05*, Pittsburgh, Pennsylvania, USA, 2005, pp. 133–139. [Online]. Available: <https://www.aaai.org/Papers/AAAI/2005/AAAI05-022.pdf>
- [37] M. Chen, H. V. Poor, W. Saad, and S. Cui, “Convergence Time Optimization for Federated Learning over Wireless Networks,” in *53rd ICC 2020*, Shanghai (China), Jul. 2020, pp. 1–6. [Online]. Available: <http://arxiv.org/abs/2001.07845>
- [38] L. Buşoniu, R. Babuška, and B. De Schutter, “Multi-agent Reinforcement Learning: An Overview,” in *Innovations in multi-agent systems and applications-1*. Springer, 2010, pp. 183–221.
- [39] S. Omidshafiei, J. Pazis, C. Amato, J. P. How, and J. Vian, “Deep Decentralized Multi-task Multi-Agent Reinforcement Learning under Partial Observability,” *34th Int. Conf. Mach. Learn. ICML 2017*, vol. 6, pp. 4108–4122, Mar. 2017.
- [40] T. D. Kulkarni, K. Narasimhan, A. Saeedi, and J. Tenenbaum, “Hierarchical Deep Reinforcement Learning: Integrating Temporal Abstraction and Intrinsic Motivation,” in *Advances in Neural Information Processing Systems 29*, D. D. Lee, M. Sugiyama, U. V. Luxburg, I. Guyon, and R. Garnett, Eds. Curran Associates, Inc., 2016, pp. 3675–3683.
- [41] S. C. Y. Chan, S. Fishman, J. Canny, A. Korattikara, and S. Guadarrama, “Measuring the Reliability of Reinforcement Learning Algorithms,” *arXiv preprint arXiv:1912.05663*, Dec. 2019. [Online]. Available: <http://arxiv.org/abs/1912.05663>
- [42] V. Mnih, K. Kavukcuoglu, D. Silver, and etc, “Human-level Control Through Deep Reinforcement Learning,” *Nature*, vol. 518, no. 7540, pp. 529–533, Feb. 2015. [Online]. Available: <https://www.nature.com/articles/nature14236>